

Corrosion Behavior of Electroless Ni-P/Ni-B Coating on Magnesium Alloy AZ91D in NaCl Environment

Jun Zhang¹, Zhengwei Song^{2,*}, Gang Yu^{1,*}, Bonian Hu³, Xueyuan Zhang¹

¹ State Key Laboratory of Chemo/Biosensing and Chemo metrics, College of Chemistry and Chemical Engineering, Hunan University, Changsha 410082, PR China

² Department of Chemistry and Chemical Engineering, Taiyuan Institute of Technology, Taiyuan 030024, PRChina

³ Department of Materials and Chemical Engineering, Hunan Institute of Technology, Hengyang 421002, PR China

*E-mail: adsszw@163.com, yuganghnu@163.com

Received: 27 August 2016 / Accepted: 13 October 2016 / Published: 10 November 2016

The Ni-P/Ni-B coating was deposited on AZ91D magnesium alloy by electroless plating. Ni-P coating as inner layer and Ni-B coating as outer layer. A tight and compact Ni-P/Ni-B coating on Mg alloy substrate was formed via Ni-P plating for 70 min and Ni-B plating for 20 min. The corrosion behavior of coating was studied by electrochemical test and neutral salt spray test in the presence of chloride environment. The test results shown that the double coating has better corrosion resistance than single Ni-P or Ni-B coating. Ni-B plated outer layer functions as cathodic protective and sealing layer, assisting Ni-P coatings in obstructing the attack of Cl⁻ in the stage of long-term immersion in NaCl solution.

Keywords: Electroless Ni-P; Electroless Ni-B; Corrosion; Mg alloy; EIS

1. INTRODUCTION

Magnesium alloys as green material have drawn wide interests. Which are intensively applied in communication, aerospace, medicine and automobile industries because of its special property, such as excellent castability, biocompatibility, and the high strength/weight ratio [1-4]. However, Mg alloys with high Mg content has high chemical reactivity lead to poor corrosion resistance, this is the main reason for limits its more widespread applications [5-7]. Therefore, corrosion and protection of magnesium alloys has been widely investigated [2, 8-10].

Although a variety of methods have been used to improve the corrosion resistance of magnesium and its alloys [11-14]. Electroless nickel (EN) plating is of special interest due to its

advantages such as uniform deposition, good corrosion and wear resistance, thermal conductivity and good electrical, and good solderability[2]. The research of EN coatings on Mg alloys was a hot topic in recent years [15-17]. However, in the process of electroless Ni-P, some pores were formed in/on the coating due to hydrogen evolution and the existence of defects on substrate. When the corrosion media through the pore and contract with substrate, Ni-P coating as cathode and Mg substrate as anode, the galvanic corrosion between Ni-P/Mg galvanic couple seems still to be a serious problem [10, 18-20].

As an effective solution, the duplex-layer or multi-layer coating was employed to improve the corrosion-resistance of the anodic substrate[21]. V. Ezhil Selvi et al [22]report that electroless Ni-P/Ni-W-P coatings on magnesium alloy AZ31B. The experimental results shown that Ni-P/Ni-W-P coating exhibited dense, less nodular and smooth appearance compare with Ni-P coating. The corrosion current of duplex Ni-P/Ni-W-P 430 times lower than Ni-P coating. These results shown that the duplex coating can improve the corrosion resistance of the AZ31B greatly more than single Ni-P coating. Shan Zhang et al[23] prepared high corrosion resistance Cu/Ni-P coating on AZ91D magnesium alloy. The Cu coating was deposited on AZ91D via HF acid pickling, Zn immersion and electrodeposition processes. Then Ni-P coating as top layer was electrodeposited on Cu coating successfully. Cu coating as an interlayer is of good adherence to AZ91D and Ni-P coatings. The corrosion test results indicated that Cu layer has positive corrosion potential functions as a cathodic protective layer, assisting Ni-P coatings in obstructing the attack of Cl^- during the anodic dissolution of Ni-P coatings in the initial stage of long-term immersion in NaCl solution.

In this paper, the Ni-P/Ni-B coating was prepared on AZ91D via electroless Ni-P and electroless Ni-B processes. The potentiodynamic polarization and electrochemical impedance spectroscopy (EIS) together with XRD and Scanning Electron Microscope (SEM) were used to research the corrosion behavior of Ni-P/Ni-B coating on Mg alloys in Cl^- environment. Aiming to establish a comprehensive model to understand their corrosion mechanisms for evaluating and monitoring the protection performance of Ni-P/Ni-B coatings on Mg alloys.

2. EXPERIMENTAL

2.1 Material preparation

AZ91D magnesium alloy (9.2wt.% Al, 0.8wt.% Zn, 0.2wt.% Mn, <0.05wt.% Si, <0.025wt.% Cu, and Mg balance) was cut into rectangular shape coupons with a size of 20×30×1.5 mm and used as the substrate for experiment. The AZ91D samples were successively polished with 300, 600 grit abrasive papers and then washed in distilled water and acetone step by step.

2.2 Coating preparation

The process flow, the main parameters for electroless Ni-P and electroless Ni-B were listed in Table 1. The specimens were cleaned with distilled water as quickly as possible between any two treatments steps. The aim of acetone cleaning and alkaline cleaning was to remove stains on the

surface of the Mg substrates. Through acid pickling, the oxides of substrate were removed and the roughness of substrate surface increased, which can increase the binding force between coating and substrate. Two steps of activation were employed to prevent Mg substrate from excessive corrosion in acid EN bath and to increase the activity of Ni electroless deposition[24]. The pretreatment of electroless Ni-P on Mg alloy was introduced in our previous studies [25-27].

Table 1. The process flow and parameters for pretreatment of AZ91D Mg alloy and electroless Ni-P and electroless Ni-B on AZ91D Mg alloy

process	Solution compositions		Conditions	
1. Acetone cleaning	Acetone		Room temperature	
2. Alkaline cleaning	NaOH	50 g·dm ⁻³	Temperature time	60 ±5 °C 8~10 min
	Na ₃ PO ₄ ·12H ₂ O	10 g·dm ⁻³		
3. Acid etching	H ₃ PO ₄	605 cm ³ ·dm ⁻³	Temperature	25 °C
	HNO ₃	30 cm ³ ·dm ⁻³	Time	30~40 s
4. First activation	K ₄ P ₂ O ₇	160 g·dm ⁻³	Temperature	70 °C
	Na ₂ CO ₃	20 g·dm ⁻³	Time	2~3 min
	KF	11 g·dm ⁻³		
5. Second activation	H ₃ PO ₄	180cm ³ ·dm ⁻³	Temperature	25 °C
	NH ₄ HF ₂	95 g·dm ⁻³	Time	2~3 min
6. Electroless Ni-P	NiSO ₄ ·6H ₂ O	20 g·dm ⁻³	Temperature	85±5 °C
	NaH ₂ PO ₂ ·H ₂ O	20 g·dm ⁻³	Time	0-90 min
	C ₆ H ₈ O ₇ ·H ₂ O	5 cm ³ ·dm ⁻³	pH	4.5-5.5
	NH ₄ HF ₂	10 g·dm ⁻³		
	CS(NH ₂) ₂	1 mg·dm ⁻³		
	HF (40%)	12 cm ³ ·dm ⁻³		
7. Electroless Ni-B	NiCl ₂ ·6H ₂ O	20 g·dm ⁻³	Temperature	80±5 °C
	NaBH ₄	0.8 g·dm ⁻³	Time	0~90 min
	C ₂ H ₈ N ₂	35 g·dm ⁻³		
	NH ₄ HF ₂	5 g·dm ⁻³		
	CS(NH ₂) ₂	1 mg·dm ⁻³		

2.3. Electrochemical measurements

The electrochemical measurements was test in NaCl solution at room temperature via Interface 1000 electrochemical workstation (Gamry Instruments, USA). The research samples as a working electrode, a Pt foil as a counter electrode and a saturated calomel electrode (SCE) as a reference electrode. The working electrodes were homemade via embedding research samples in epoxy resin, and the surface with a 10×10 mm² area was exposed as effective working side. [10].

Electrochemical impedance spectroscopy (EIS) measurements were tested after exposing the specimens to the electrolyte for different time over a frequency range from 100000 to 0.01 Hz at the open circuit potential with an AC amplitude of 10 mV. Potentiodynamic polarization measurements were carried out in the potential region from the open circuit potential to ± 500 mV with a potential scanning rate $1 \text{ mV}\cdot\text{s}^{-1}$ from cathodic to anodic. For each specimen, the measurements were replicated at least three times to ascertain reproducibility and one of the results was chosen as a representative to present in this work.

2.4. Surface morphologies characterization

The metallurgical microstructure, cross-section microstructure, corrosion morphologies as well as elemental composition of the specimens were characterized by JSM-561(Seiko Instruments Inc. Japan) scanning electron microscope (SEM) equipped with an energy-dispersive spectrometer (EDS). The crystal structure of different coating and substrate were analyzed by X-ray diffraction (XRD, SHIMADZU-6100, Japan) using a Cu target.

2.5 Adhesion test

The adhesion between the coating and the substrate was tested by thermal shock method according to ASTM B 733-04[18]. The prepared samples were heated to 220 ± 10 °C for 1 h and quickly quenched at room temperature water. The heating and quenching of samples were carried out for 20 cycles. Then the adhesion of the coating was evaluated for blistering, broken off, crinkle and other evidence of poor adhesion at 4 times magnification.

2.6 Neutral Salt spray test

The NSST samples were exposed to a 5 wt% NaCl solution and the temperature was 35 ± 2 °C. The environment conducted as ASTM B117-07 standard. In each case, three samples were tested, and the average values were the final results.

3. RESULTS AND DISCUSSION

3.1 Plating process

The process flow and parameters were listed in Table 1. According to recent report[28], electroless Ni-P coating has some pores when the plating time less than 90 min. The corrosion resistance of coatings with different electroless Ni-P and Ni-B plating time were investigated when the whole plating time was 90 min. The polarization curves for various kinds of coating in 3.5 wt. % NaCl for 8 h were shown in Figure 1. Curve 1 in Figure 1 was the coating obtained via electroless Ni-P plating for 10 min and electroless Ni-B plating for 80 min, Curve 2 was the coating obtained via electroless Ni-P plating for 20 min and electroless Ni-B plating for 70 min. And so on, Curve 8 was the

coating obtained via electroless Ni-P plating for 80 min and electroless Ni-B plating for 10 min. Electrochemical parameters such as corrosion current (i_{corr}), corrosion potential (E_{corr}), cathodic Tafel slopes (b_c) and anodic Tafel slopes (b_a) were derived from the polarization curves by Tafel extrapolation[18]. On the basis of these parameters, the polarization resistance (R_p) value was inversely proportional to the corrosion rate and determined by the simplified Stern-Geary relationship (Eq. (1)):

$$R_p = \frac{b_a \cdot b_c}{2.303 i_{corr} (b_a + b_c)} \quad (1)$$

The values of electrochemical corrosion parameters were shown in Table 2. The results shown that the coating prepared via electroless Ni-P plating for 70 min and electroless Ni-B plating for 20 min (coating 7) has higher corrosion resistance than other coating. In contrast with other coating, it shows a higher corrosion potential (-0.3197 V_{SCE}) and a lower corrosion current density ($1.34 \times 10^{-6} \text{ A}\cdot\text{cm}^{-2}$) after immersion in 3.5 wt.% NaCl solution for 8 h. The corrosion potentials and corrosion current densities of coatings except coating 7 were similar with each other. It also indicated that these coatings were corroded and the corrosive media penetrates through coating and contacts with Mg alloy substrate. In this paper, Coating 7 was chosen as sample for following research.

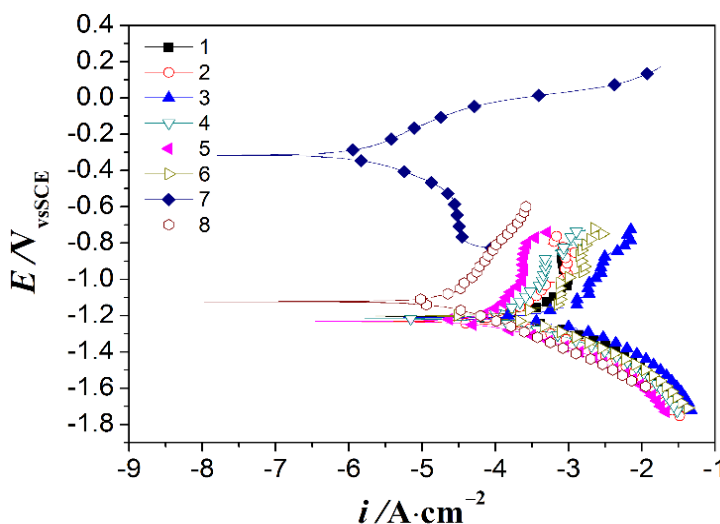


Figure 1. The Polarization curve of different coatings immersion in 3.5% NaCl solution for 8 h

Table 2. The value of electrochemical parameters obtained from polarization curves in Figure 1

sample	$E/(V_{SCE})$	$i/(A\cdot cm^{-2})$	$b_a/(mV\cdot dec^{-1})$	$b_c/(mV\cdot dec^{-1})$	$R_p/(\Omega\cdot cm^2)$
1	-1.207	4.65×10^{-4}	293	234	111
2	-1.236	1.84×10^{-4}	259	169	241
3	-1.230	9.55×10^{-4}	553	202	67
4	-1.231	2.12×10^{-4}	529	161	252
5	-1.203	7.39×10^{-5}	467	149	663
6	-1.216	3.07×10^{-4}	377	189	178
7	-0.318	1.34×10^{-6}	180	155	26987
8	-1.124	2.39×10^{-5}	486	166	2248

3.2 Structure of coating

The surface SEM and EDS of Ni-P coating for 70 min plating were shown in Figure 2. The coating is uniform, and shows a typical nodular structure which is common for electroless Ni-P coating[15]. The nodular size of Ni-P coating is about 5-10 μm . As shown in Figure 2a, the coating has high density, low porosity and smooth surface structure. The EDS result shows that the P content of the Ni-P coating surface is about 11 wt.%. It means that Ni-P coating is amorphous and exhibits good corrosion resistance[29].

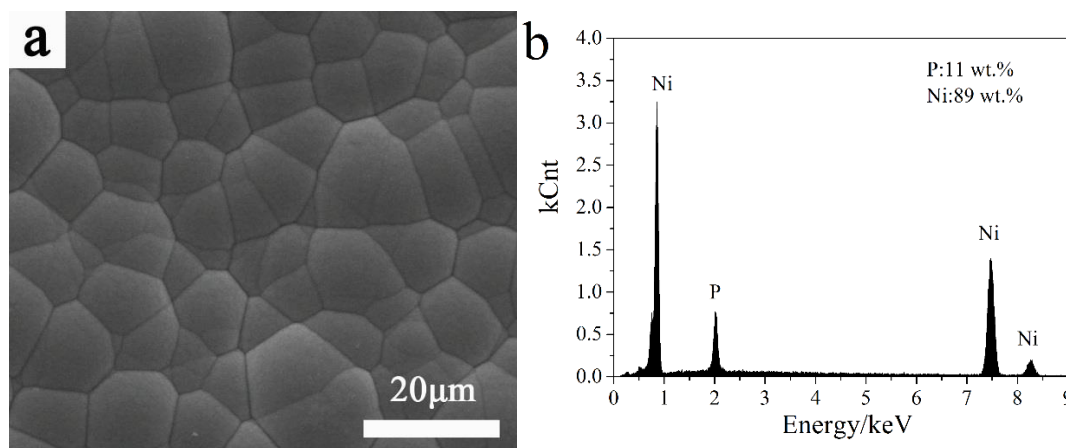


Figure 2. The surface morphology and EDS of Ni-P coating for 70 min electroless plating a: surface morphology b:EDS

The SEM figures of Ni-P/Ni-B coating surface and cross section are shown in Figure 3a and Figure 3b. It shows that the coating surface exhibited nodular structure (in Figure 3a). These nodules are continuous and no pore is visible between these clusters of nodules. The average diameter of these cluster nodules is about 10 μm . There are no double-layer structure exhibits in Figure 3b. It indicate that the excellent adhesion between inner Ni-P and outer Ni-B layer. There are metal bond and sintered interlocking between the Ni-P/Ni-B and Mg alloy substrate. No blistering, crinkle, broken off were observed at 4 times magnification after 20 cycles of thermal shock experiment according to ASTM B733-04. This results show that the adhesion of composite coating is excellent. Figure 3c shows the EDS of double coating. There are no other elements peak shown in EDS except Ni, no B element was detected due to small molecular weight and less content of B. So the possible boundary between the Ni-P bottom layer and outer Ni-B layer can be speculated according to the linear distribution of phosphor element. Figure 3d shows the linear scanning of the elements from Ni-P/Ni-B coating to Mg alloy substrate. The thickness of coating about 16 μm . The curve of P content shows that the thickness of Ni-P coating about 14 μm and Ni-B layer about 2 μm . The 14 μm Ni-P layer mainly contains Ni and P. The P distribution was not equal in the coating, higher P element near to coating surface and lower P element near to the substrate. Because the pH of plating solution was decreased with prolonging plating time. Lower phosphorus content Ni-P coating was obtained in high pH values solution, whereas high phosphorus Ni-P coating was plated in low pH bath contain [30-32].

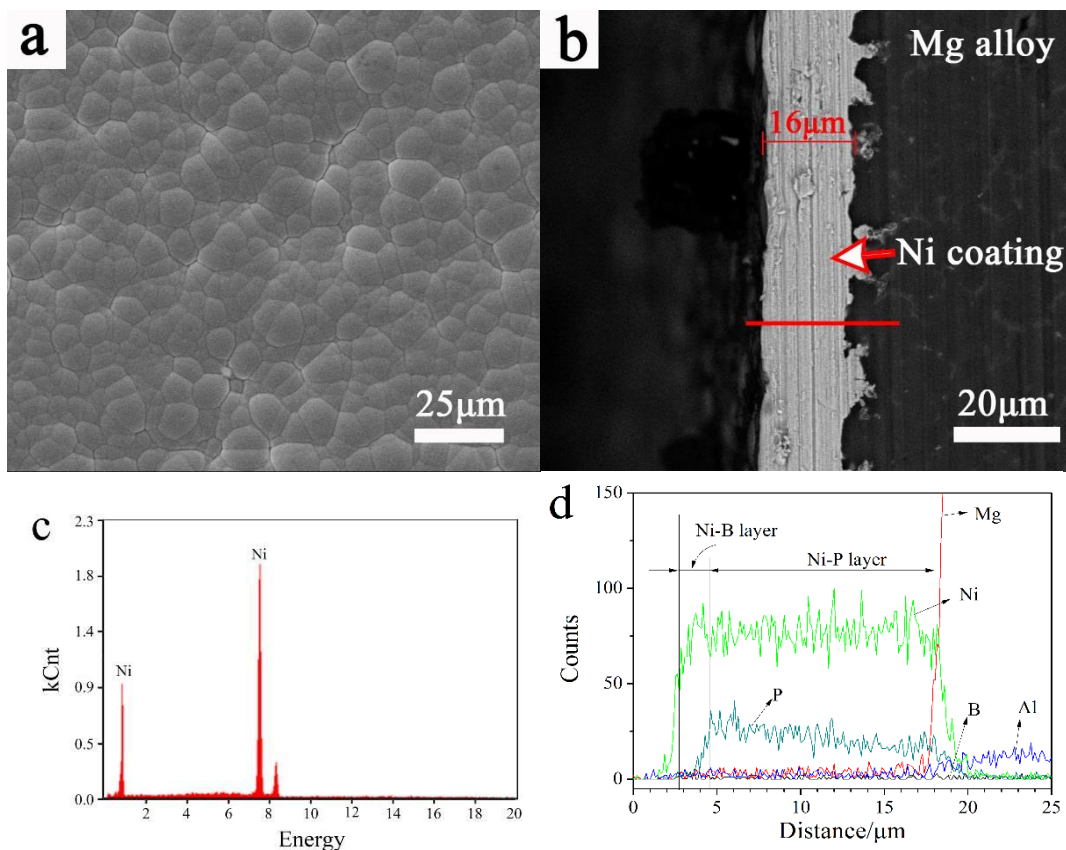


Figure 3. Coating structure and elements content a: surface morphology; b: cross section; c:EDS of surface; d: linear scanning of elements

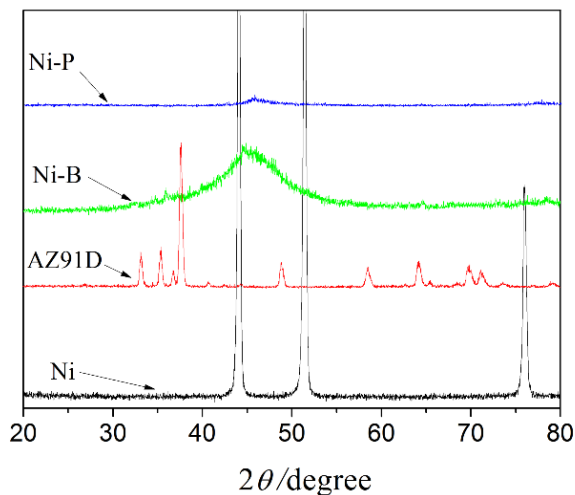


Figure 4. XRD curves of Ni, AZ91D, Ni-P and Ni-P/Ni-B

Figure 4 displays the XRD patterns of Ni, AZ91D and electroless Ni-P coating, electroless Ni-B coating on Ni-P surface. It is clearly that three diffraction peaks of Ni at $2\theta = 44.51^\circ$, 52.00° and 76.57° , respectively, correspond to the characteristic peaks of the Ni(111), Ni(200) and Ni(220) planes of the face-centered cubic Ni crystals (JCPDS Card No. 04-0850)[33]. After electroless Ni-B or Ni-P plating, the lattice distortion leading to the main diffraction peak of nickel broaden and gradually

weaken was due to the P or B atoms into the face-centered cubic lattice of nickel. The Ni-P coating with high P content shows a wide and weak peak of Ni (111), which is an evidence of amorphous structure[34]. Ni-B coating presents a wide peak, but the peak intensity is higher than Ni-P coating. It indicate that the Ni-B coating has amorphous structure which not only packed with Ni element also has B element, but exhibit a low non-crystallizing degree than Ni-P. The Ni-P coating with high non-crystallizing degree performed higher corrosion resistance than Ni-B[35].

3.3 Open circuit potential

Open circuit potential curves of Ni-B, Ni-P and Ni-P/Ni-B coating coated on Mg alloy in NaCl solution are shown in Figure 5. The OCP of Ni-B coating coated Mg alloy sample first increases from -0.42 to -0.32 V_{SCE} during the initial 2000 s. indicating passivation layer were formed on the surface of Ni-B. The open circuit potential decreased rapidly from -0.32 to -1.25 V_{SCE} after 60 min immersion, a large amount of hydrogen evolution from the sample was observed with the naked eye. It indicated some place of coating destroyed and the corrosion solution through the coating contact with substrate, the galvanic coupling had set up. The potential of Ni-P increase first and then reach a steady potential (from -0.34 to -0.32 V_{SCE}) within initial 326 min, it indicated that passivation layer formed on Ni-P coating immersion in NaCl solution[23]. The open circuit potential decreased rapidly from -0.32 to -1.22 V_{SCE} after 326 min. The electrolyte with 3.5 wt.% NaCl had to penetrate into the pores of Ni-P coating and contact with substrate, the galvanic coupling had set up. The potential of Ni-P/Ni-B coating coated sample first decrease from -0.24 V_{SCE} to -0.28 V_{SCE} during the initial 23 min, then reached a stable potential stage.

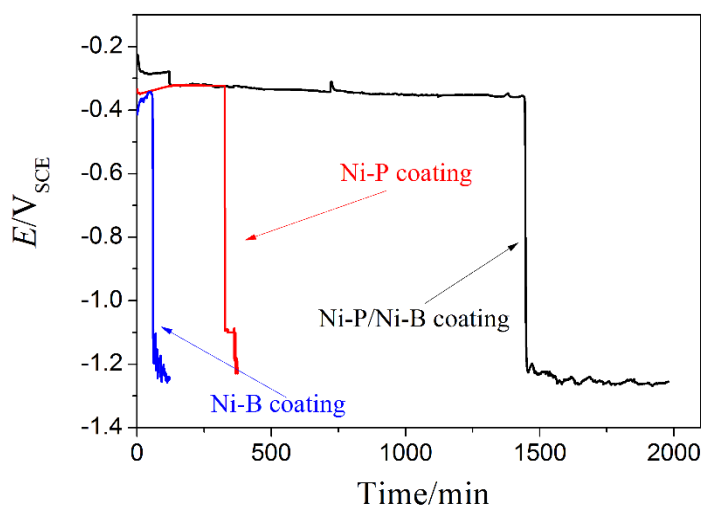


Figure 5. OCP curves of different coating in NaCl solution

As immersion time prolonged, the open circuit potential decreased rapidly from -0.28 to -0.32 V_{SCE} after 120 min. It indicated the coating was dissolved in NaCl solution. The potential decreased slowly from -0.32 to -0.35 V_{SCE} in the range of 120-1440 min. And it decreased rapidly from -0.35 V_{SCE} to -1.22 V_{SCE} after 1440 min. In the initial stage of immersion, the OCPs of Ni-P and Ni-B are

lower than Ni-P/Ni-B. It indicated that the double coating has more compact structure than single coating, which has better barrier performance against NaCl solution permeation. The results of OCP curves in Figure 5 indicate that the Ni-P/Ni-B layer is more thermodynamically steady than Ni-B or Ni-P in NaCl solution.

The surface morphology and EDS of Ni-P coating after immersion in NaCl solution for 8h were shown in Figure 6. Figure 6a shows that some corrosion pits were formed on Ni-P coating, but unevenly distributed in the whole surface, which indicated that local corrosion occurred. The EDS result in the pit area was shown in Figure 6b. The content of P in the coating after corrosion was higher than uncorrupted coating (in Figure 2b). It suggests that some Ni atoms on Ni-P coating surface were dissolved in NaCl solution and result in gradual accumulation of the P content.

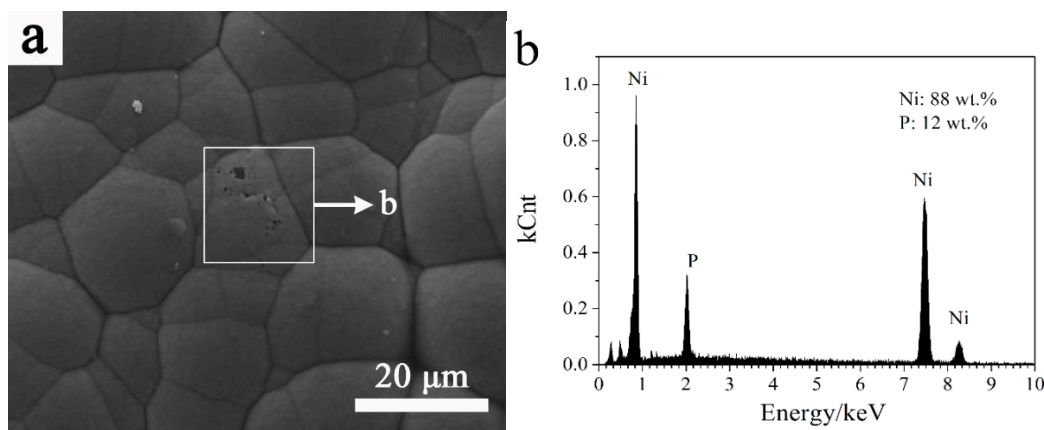


Figure 6. surface morphology and EDS of Ni-P coating after immersion in NaCl solution for 8h
a:surface Morphology b:EDS

3.4 EIS characteristics

The corrosion behavior of Ni-P/Ni-B coating in 3.5 wt.% NaCl solution was monitored by EIS spectra. The EIS spectra of Ni-P/Ni-B coatings in NaCl solution for long-term immersion were shown in Figure 7. The Nyquist plots and Bode plots were presented in Figure 7(a) and (b), respectively. In order to further understand the corrosion mechanisms, the corresponding equivalent circuits for EIS tests of the immersion samples are shown in Figure 7c and 7d. From Figure 7a, In the case of the sample with different immersion time in the range of 2-23 h, only a capacitance loop was observed and the EIS spectra were similar except for the difference in the diameter of the loops. The EIS plots could be well fitted by the equivalent circuit shown in Figure 7c. Two capacitance loops were observed in EIS of the sample after 33 h immersion. The EIS plots could be well fitted by the equivalent circuit shown in Figure 7d. The plots are fitted using Zsimpwin 3.10 software and the results are listed in Table 3. The resistance increased gradually with increase of immersion time in the range of 2-6 h, and then decreased when the immersion time to 10 h. It indicates the corrosion resistance of Ni-P/Ni-B coatings first increases and then decreases during immersion in NaCl solution in the range of 2-10 h. The resistance increases to the maximum after 20 h immersion and then becomes small. The change of EIS curves of Ni-P/Ni-B indicated that the corrosion of double coating has three steps. In the first step,

the dissolution of the nickel atom on Ni-B coatings surface in the NaCl media resulting in gradual accumulation of the B content, the Ni-B coatings is passivation in the initial immersion stage. This phenomenon was also shown in the results of OCP test (Figure 5). In the second step, the corrosion solution has permeated through outer layer and contacted with inner layer, the amorphous structure of Ni-P lead to coating compactly, and higher P content in Ni-P layer resulting in high P passivation layer formed on Ni-P surface in NaCl solution[23], so Ni-P was corroded slowly in this stage. The third stage was the immersion time after 33 h in which visible corrosion pits were observed. Once the corrosion pits penetrate the coatings, serious galvanic corrosion will destroy the substrate quickly. Accordingly, the corrosion resistance of Ni-P/Ni-B coatings exists two maximum values in the stage of the long-term immersion in NaCl solution. As the standard electrode potential of Ni-P is higher than that of Ni-B alloys, the Ni-B as out layer can assisting Ni-P coatings in obstructing the attack of Cl⁻ during the anodic dissolution of Ni-B coatings.

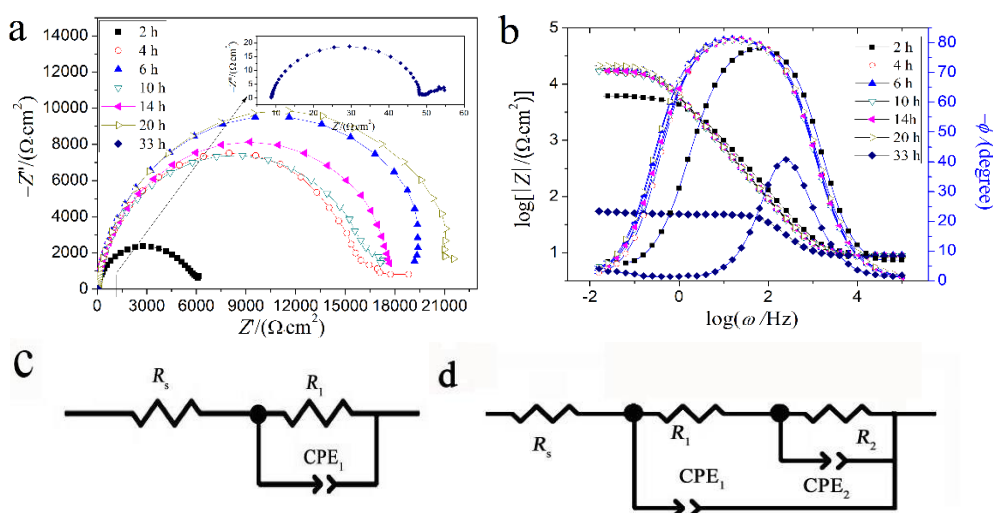


Figure 7. EIS plots of coating coated AZ91D in 3.5 wt.% NaCl solution for different time a: Nyquist plots; b: bode plots; c and d: equivalent circuits

Table 3. Estimated elements of the equivalent circuit through fitting the EISs (referring to Figure 7)

	$R_s/\Omega \cdot \text{cm}^2$	$Y_1/\text{S} \cdot \text{sec}^n \cdot \text{cm}^{-2}$	n_1	$R_1/\Omega \cdot \text{cm}^2$	$Y_2/\text{S} \cdot \text{sec}^n \cdot \text{cm}^{-2}$	n_2	$R_2/\Omega \cdot \text{cm}^2$
2 h	8.96	$2,22 \times 10^{-5}$	0.91	5747	-	-	-
4 h	9.11	2.67×10^{-5}	0.93	16350	-	-	-
6 h	9.14	2.78×10^{-5}	0.93	20700	-	-	-
10 h	8.92	3.02×10^{-5}	0.93	16730	-	-	-
14 h	8.81	2.87×10^{-5}	0.93	18170	-	-	-
20 h	8.39	2.87×10^{-5}	0.93	22190	-	-	-
33 h	8.81	5.47×10^{-5}	0.95	39.84	0.40	0.69	9.53

The morphology and component of double coating after electrochemical polarization test was investigated for intuitive understanding its corrosion behavior. The cross section and EDS of double

coating after electrochemical polarization test were shown in Figure 8. The corrosion hole shaped like a bowl with a large opening at the top and a slightly smaller opening at the bottom (as shown in Figure 8a). P element was detected at bottom of corrosion hole by EDS. The corrosion media through Ni-B coating and contact with Ni-P coating and the corrosion of Ni-P coating was occurred. The shape of corrosion hole suggest that the corrosion of Ni-B coating in preference to Ni-P coating. The released electrons of Ni-B would transfer from Ni-B to Ni-P, which will decrease the corrosion rate of Ni-P.

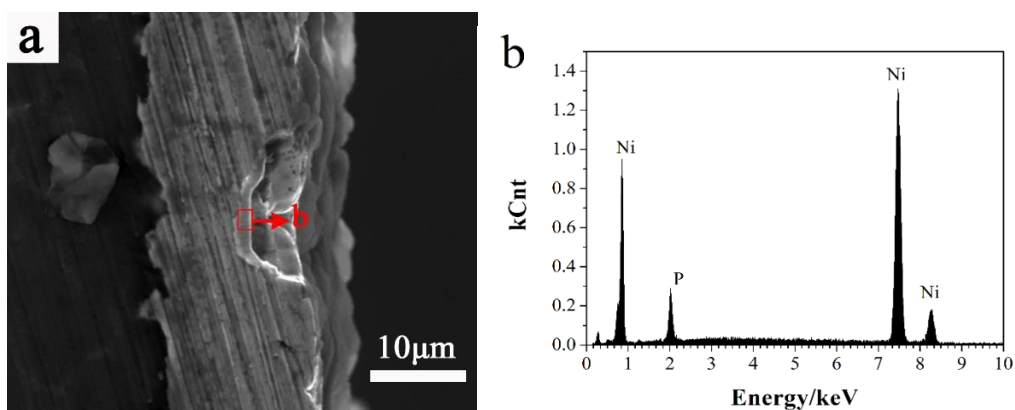


Figure 8. Cross section and EDS of double coating after electrochemical polarization test in NaCl solution a: cross section b: EDS

3.5 Neutral salt spray test

The surface morphology and EDS of Ni-P/Ni-B coating coated Mg alloy after neutral salt spray test for 50 h were shown in Figure 9. There was no noticeable corrosion pits on the surface of the Ni-P/Ni-B coated AZ91D alloy by naked eyes until neutral salt spray testing for 50 h. It indicated that the coating could provide good protection for Mg alloy substrate.

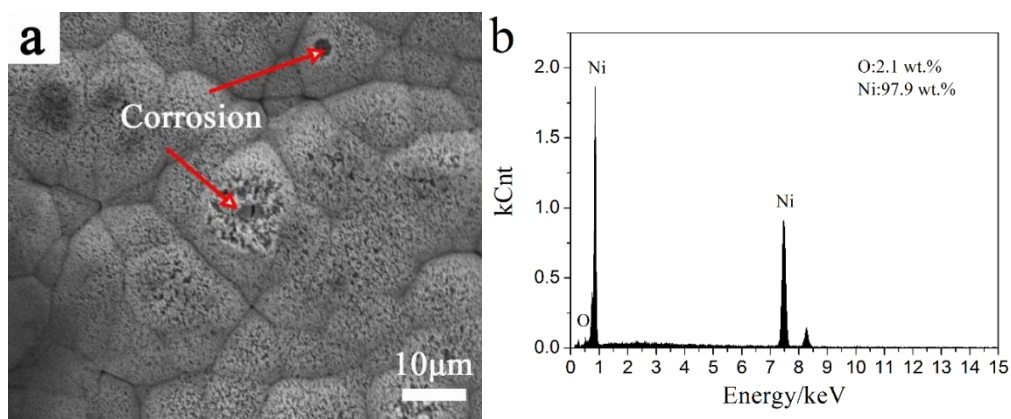


Figure 9. The surface morphology and EDS of coating after neutral salt spray test for 50 h a and b: SEM; c: EDS

Figure 9a shown that the corrosion of Ni-P/Ni-B was actually occurred after 50 h test, the outer layer was corroded. The EDS of corrosion hole was shown in Figure 9b, the results shown that the corrosion products were comprised of Ni and O. no P and Mg elements. It also indicated that the substrate was not corroded.

3.6 Corrosion model

The corrosion model of Ni-P/N-B and single Ni-P, Ni-B coating coated Mg alloy (as shown in Figure 10) were obtained according to experimental results. According to the atomic hydrogen theory of electroless nickel-plating, the hydrogen evolution was simultaneous the deposition of Ni with in the process of electroless Ni-P and Ni-B plating. So some defects such as pores were formed in the coating growth process. When the corrosion occurs on Mg alloy with single Ni-P or Ni-B layer, the NaCl solution penetrating the coating in the defect place and contract with Mg alloy substrate finally(as shown in Figure 10). The average thickness of coating in defect place was thinner than other place, so the through hole was prone to formation in defect place when corrosion occurred, the corrosion cell was formed with Ni-B or Ni-P coatings as cathode part and Mg alloy as anode part.

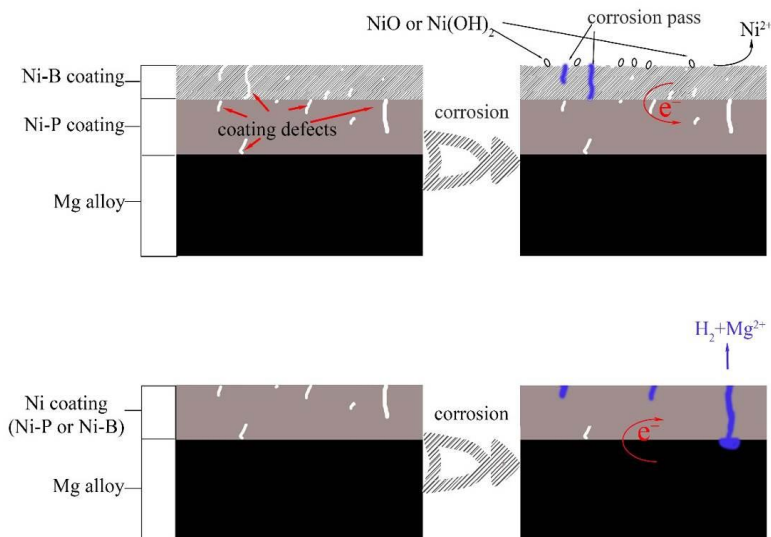


Figure 10. Corrosion model of coating

When the corrosion occurs on Mg alloy with Ni-P/Ni-B coating, Ni-B was served as outer layer which have the functions of sealing and cathode protection. Firstly, Ni-B are preferentially nucleated on scratches and defects on the Ni-P surface in the process of electroless Ni-B plating[36], therefore, Ni-B layer as sealing coating can prevent the corrosion solution contact with substrate through Ni-P coating defects. Even if penetrating holes developed in the outer layer, the chance of the corrosive media reaching the substrate is small due to mismatch of coating defects in two layers. Secondly, the outer Ni-B layer with low corrosion potential corroded preferentially to the inner Ni-P layer with high corrosion potential, which could delay the corrosion process of Ni-P coating. Thirdly, According to the

literature, Ni-B coating exhibit higher hardness than Ni-P coating[37]. Hard outer layer can provides excellent mechanical protection for inner layer[28]. Therefore, Ni-P/Ni-B coating can provide better protection than single Ni-P or Ni-B layer in the practical application.

4. CONCLUSIONS

The Ni-P/Ni-B coating obtained via 70 min electroless Ni-P plating and 20 min electroless Ni-B plating has higher corrosion resistance. The thickness of the Ni-P/Ni-B coating was about 16 μm , Ni-P about 14 μm and Ni-B about 2 μm . Both Ni-P and Ni-B have amorphous structure. The Ni-P coating with high non-crystallizing degree performed higher corrosion resistance and corrosion potential than Ni-B. The corrosion resistance of Ni-P/Ni-B was higher than single Ni-P or Ni-B coating. Ni-B was served as outer layer which have the functions of sealing and cathode protection. The outer Ni-B layer with low corrosion potential corroded preferentially to the inner Ni-P layer with high corrosion potential, which could decrease the corrosion rate of Ni-P to some extent.

ACKNOWLEDGEMENT

This study is jointly funded by the National Natural Science Foundation (21176061), the Key Natural Science Foundation (12JJ2006) and the Construct Program of Key Disciplines in Hunan Province.

References

1. Y. Liu, X. Yin, J. Zhang, S. Yu, Z. Han, L. Ren, *Electrochim. Acta*, 125 (2014) 395-403.
2. L.L. Wang, H.J. Chen, W.Q. Huang, L. Hao, *Surf. Eng.*, 25 (2009) 376-381.
3. N. Kamiyama, G. Panomsuwan, E. Yamamoto, T. Sudare, N. Saito, T. Ishizaki, *Surf. Coat. Technol.*, 286 (2016) 172-177.
4. J.E. Gray, B. Luan, *J. Alloys Compd.*, 336 (2002) 88-113.
5. A. Abdal-hay, M. Dewidar, J. Lim, J.K. Lim, *Ceram. Int.*, 40 (2014) 2237-2247.
6. T.S.N. Sankara Narayanan, I.S. Park, M.H. Lee, *Prog. Mater Sci.*, 60 (2014) 1-71.
7. S. Agarwal, J. Curtin, B. Duffy, S. Jaiswal, *Mater. Sci. Eng., C*, (2016).
8. A. Atrens, N. Winzer, W. Dietzel, *Adv. Eng. Mater.*, 13 (2011) 11-18.
9. R.-c. Zeng, J. Zhang, W.-j. Huang, W. Dietzel, K.U. Kainer, C. Blawert, W. Ke, *Trans. Nonferrous Met. Soc. China*, 16, Supplement 2 (2006) s763-s771.
10. Z. Song, Z. Xie, G. Yu, B. Hu, X. He, X. Zhang, *J. Alloys Compd.*, 623 (2015) 274-281.
11. N. Kamiyama, G. Panomsuwan, E. Yamamoto, T. Sudare, N. Saito, T. Ishizaki, *Surf. Coat. Technol.*, 286 (2016) 172-177.
12. C. Gu, W. Yan, J. Zhang, J. Tu, *Corros. Sci.*, 106 (2016) 108-116.
13. Y. Mori, A. Koshi, J. Liao, *Corros. Sci.*, 104 (2016) 207-216.
14. M.-J. Wang, S.-C. Chao, S.-K. Yen, *Corros. Sci.*, 104 (2016) 47-60.
15. Y. Zou, Z. Zhang, S. Liu, D. Chen, G. Wang, Y. Wang, M. Zhang, Y. Chen, *J. Electrochem. Soc.*, 162 (2015) C64-C70.
16. S. Sadreddini, Z. Salehi, H. Rassaie, *Appl. Surf. Sci.*, 324 (2015) 393-398.
17. Y. Mao, Z. Li, K. Feng, X. Guo, Z. Zhou, J. Dong, Y. Wu, *Appl. Surf. Sci.*, 327 (2015) 100-106.
18. L. Zeng, S. Yang, W. Zhang, Y. Guo, C. Yan, *Electrochim. Acta*, 55 (2010) 3376-3383.

19. J. Calderón, J. Jiménez, A. Zuleta, *Surf. Coat. Technol.*, (2016).
20. D. Seifzadeh, L. Farhoudi, *Surf. Eng.*, 32 (2016) 348-355.
21. M. Rezagholizadeh, M. Ghaderi, A. Heidary, S.M.M. Vaghefi, *Prot. Met. Phys. Chem*, 51 (2015) 234-239.
22. V.E. Selvi, P. Chatterji, S. Subramanian, J.N. Balaraju, *Surf. Coat. Technol.*, 240 (2014) 103-109.
23. S. Zhang, F. Cao, L. Chang, J. Zheng, Z. Zhang, J. Zhang, C. Cao, *Appl. Surf. Sci.*, 257 (2011) 9213-9220.
24. D. Yan, G. Yu, B. Hu, J. Zhang, Z. Song, X. Zhang, *J. Alloys Compd.*, 653 (2015) 271-278.
25. Y. Zhu, G. Yu, B. Hu, X. Lei, H. Yi, J. Zhang, *Appl. Surf. Sci.*, 256 (2010) 2988-2994.
26. R. Sun, G. Yu, Z. Xie, B. Hu, J. Zhang, X. He, X. Zhang, *Int. J. Electrochem. Sci.*, 10 (2015) 7893-7904.
27. Z. Xie, G. Yu, B. Hu, X. Zhang, L. Li, W. Wang, D. Zhang, *Int. J. Electrochem. Sci.*, 8 (2013) 6664-6677.
28. X. Shu, Y. Wang, C. Liu, A. Aljaafari, W. Gao, *Surf. Coat. Technol.*, 261 (2015) 161-166.
29. P.-H. Lo, W.-T. Tsai, J.-T. Lee, M.-P. Hung, *Surf. Coat. Technol.*, 67 (1994) 27-34.
30. A.W. Goldenstein, W. Rostoker, F. Schossberger, G. Gutzeit, *J. Electrochem. Soc.*, 104 (1957) 104-110.
31. S.L. Chow, N.E. Hedgecock, M. Schlesinger, J. Rezek, *J. Electrochem. Soc.*, 119 (1972) 1614-1619.
32. K. Sugita, N. Ueno, *J. Electrochem. Soc.*, 131 (1984) 111-114.
33. Z. She, Q. Li, Z. Wang, L. Li, F. Chen, J. Zhou, *Chemical Engineering Journal*, 228 (2013) 415-424.
34. Z. Bangwei, X. Haowen, *Mater. Sci. Eng., A*, 281 (2000) 286-291.
35. H. Ashassi-Sorkhabi, S.H. Rafizadeh, *Surf. Coat. Technol.*, 176 (2004) 318-326.
36. E. Correa, A. Zuleta, L. Guerra, M. Gómez, J. Castaño, F. Echeverría, H. Liu, A. Baron-Wiecheć, T. Hashimoto, P. Skeldon, *Surf. Coat. Technol.*, 232 (2013) 784-794.
37. W.X. Zhang, Z.H. Jiang, G.Y. Li, Q. Jiang, J.S. Lian, *Appl. Surf. Sci.*, 254 (2008) 4949-4955.